SPE COMPOSITES

SUMMER 2026

Composites Connection™

Official Newsletter of the SPE Composites Division

Reaching Over 1,000 Composites Professionals
In All Industries

Sponsored by:

AOC Trusted Solutions

BASF We create chemistry

DSC CONSUMABLES incorporated Est. 2012 Austin, MN

MICHELMAN

MITSUBISHI CHEMICAL GROUP

MP Molding Products

vartega

BASF
We create chemistry

Design sustainable, lightweight parts with composite materials

Metals have you down? Design sustainable, lightweight parts with composite technology solutions by BASF. From straight or curved profiles to prototype production, our solutions provide:

- High strength-to-weight ratios
- Highly customizable materials
- Excellent impact properties
- Cost-effective solutions due to lower manufacturing cycle times

Learn more about BASF's composite technology solutions at https://on.basf.com/Composites-Technology

SPE COMPOSITES
SUMMER 2026

Composites Connection™
Advancing Composites Technology Worldwide

Chairman's Message:

Dale Brosius

Dear Composites Division members,

Early March was a busy time in composites as both SPE ANTEC and JEC World occurred in the same week. The Composites Division, under the guidance of Alex Kravchenko, conducted two well-attended sessions, containing 12 technical papers on important topics at ANTEC in Pittsburgh on March 11-12. Concurrently, I and several other Composites Division members were in Paris at the annual JEC World event, which attracted roughly 50,000 visitors to see the latest and greatest in composites materials and manufacturing technologies on display. I came away excited for the trajectory of the industry, especially the continued thrust of sustainability.

Your Board of Directors has also evolved in March. Rich Caruso, a long-time BOD member and a multiple session chair of ANTEC as well as other roles, has elected to resign from the board yet remains very active in SPE. He also is very active in SAMPE and will continue to be a liaison between the two societies. I thank Rich for his long service. On the flip side, we have added two board members as of our March meeting. Creig Bowland, a former Chair and Councilor of the Composites Division, has returned to the BOD after a hiatus to serve other priorities. Welcome back, Creig. We also welcome Dr. Sarah Simon of Netsch as a new board member of the division. Sarah has been very active in SPE for years, first as a student member at University of Wisconsin, where she won multiple ACCE poster awards and SPE scholarships, and now as a professional member. We are pleased to have her on board.

In October 2025, SPE headquarters announced a merger of the Society with the Plastics Industry Association (PIA), the leading trade association representing plastic materials. In the merger, SPE becomes a division of PIA, with continuing missions in education and professional development. In a recent update, much of the integration of functional operations has completed, and we will see over the next months what benefits the merger will have on our division and our members, Stay tuned.

The next, and 26th edition of the SPE Automotive Composites Conference and Exhibition will be held September 9-10, 2026 at its traditional home in Novi, Michigan. The event promises to once again deliver great content, novel insights, robust discussions and ample time for networking with fellow composites enthusiasts. We are currently accepting abstracts, so I encourage you to submit your latest innovations or research. Also, please consider being a sponsor and exhibitor at the conference. All net proceeds of the conference go to furtherance of educational support for students and professionals. Go to https://speautomotive.com/acce-conference/ for more information on sponsorship and links to submit abstracts.

Best regards,
Dale Brosius
Chair, SPE Composites Division

SPONSOR LINKS

AOC Trusted Solutions

BASF We create chemistry

DSC CONSUMABLES incorporated Est. 2012 Austin, MN

MICHELMAN

MITSUBISHI CHEMICAL GROUP

MP Molding Products

vartega

MITSUBISHI CHEMICAL GROUP

Large Composite Parts for Tomorrows Mobility Design

Lightweight | Durable | Environmentally Friendly

55TH-ANNUAL

SPE AUTOMOTIVE INNOVATION AWARDS COMPETITION & GALA

HONORING THE BEST IN AUTOMOTIVE PLASTICS

NOVEMBER 4, 2026

Plastics: THE ROAD TO INNOVATION

CALL FOR NOMINATIONS

MOST INNOVATIVE USE OF PLASTICS AWARDS

The Automotive Division of the Society of Plastics Engineers (SPE®) is announcing a "Call for Nominations" for its **55TH-Annual Automotive Innovation Awards Gala,** the oldest and largest recognition event in the automotive and plastics industries. This year's Awards Gala will be held Wednesday, **NOVEMBER 4, 2026** at the **Laurel Manor** in Livonia, Michigan. Winning part nominations in 10 different categories, and the teams that developed them, will be honored with a **Most Innovative Use of Plastics** award. A **Grand Award** will be presented to the winning team from all category award winners.

SPONSORSHIP OPPORTUNITIES This annual event currently draws over 600 OEM engineers, automotive and plastics industry executives, and media. A variety of sponsorship packages - including tables at the banquet, networking receptions, advertising in the program book, signage at the event and more are available. Contact Teri Chouinard of Intuit Group at **intuitgroup@gmail.com.**

For more info and to submit nominations, go to:
https://speautomotive.com/spe-automotive-div-innovation-awards/

CATEGORIES:

- AFTERMARKET & LIMITED EDITION VEHICLES
- BODY INTERIOR
- BODY EXTERIOR
- CHASSIS/HARDWARE
- SUSTAINABILITY
- PROCESS, ASSEMBLY AND ENABLING TECHNOLOGIES
- SAFETY
- POWERTRAIN
- ELECTRIC AND AUTONOMOUS VEHICLE SYSTEMS
- MATERIALS

THANK YOU TO OUR 2025 SPONSORS

GALA, VIP RECEPTION & AFTERGLOW SPONSOR

Celanese — The chemistry inside innovation™

MAIN EVENT RECEPTION SPONSOR

BASF — We create chemistry

GOLD SPONSOR

American Chemistry Council — Plastics Division

BRONZE SPONSORS

3M Science. Applied to Life.™

covestro

elringklinger

Omya Performance Polymer Distribution

sabic

ADVERTISING SPONSOR

NIFCO

MEDIA / ASSOCIATION SPONSORS

AM Additive Manufacturing · Automotive Engineering · CW CompositesWorld · Gardner Business Media, Inc. · SPE Plastics Engineering · Plastics News · PT Plastics Technology · SAE International · Truck & Off-Highway Engineering · Urethanes Technology International

THE OLDEST AND LARGEST RECOGNITION EVENT IN THE AUTOMOTIVE & PLASTICS INDUSTRIES

The Power of SPE Composites

Tap into the power of SPE Composites' members reach! Find where we are spread across the US and the rest of the world.

SPE Composites Nation Wide

SPE Composites Worldwide

This Issue:

- Message from the Chair
- Call for Nominations
- SPE Composites Reach
- ACCE Call for Papers
- ACCE Award Paper
- TopCon 2026
- BOD Listings

Sponsor the Newsletter

The Best Advertising Value in the Composites Industry

Contact: Teri Chouinard CBC, APR
Teri@IntuitGroup.com

See page 19 for more details

AUTOMOTIVE COMPOSITES CONFERENCE & EXHIBITION

Novi, MI • September 9-10, 2026

Presented by SPE Automotive and Composites Divisions

WORLD'S LEADING AUTOMOTIVE COMPOSITES FORUM

COMPOSITES: ADVANCING MOBILITY

POLYMER COMPOSITES are advancing all forms of transportation today and into the future.

Design flexibility, lightweight, structural and other inherent benefits of composites make it the premier material for EV and all mobility applications.

CALL FOR PAPERS, SPONSORS & EXHIBITORS

PRESENT YOUR TECHNOLOGIES that are advancing the industry at ACCE 2026. Topics include: Composites in Electric Vehicles; Advances in Thermoplastic Composites; Advances in Thermoset Composites; Additive Manufacturing & 3D Printing; Enabling Technologies; Sustainable Composites; Bonding, Joining & Finishing; Carbon Composites & Reinforcements; AI (Artificial Intelligence), ML (Machine Learning) and Data-Driven Solutions; Design, Modeling and Simulation of Composites; and Composites in eVTOLs. Those interested in presenting are encouraged to send Titles and/or Topics to **intuitgroup@gmail.com. ABSTRACTS** are due **April 26, 2026** and **FINAL PAPERS AND/OR PRESENTATIONS** are due **June 28, 2026.**

SPONSORSHIP & EXHIBIT OPTIONS offer companies the opportunity to support the event and promote their products and services to a very targeted and interested OEM audience.

Automotive, Heavy Truck and other Transportation OEMs are Invited to Attend ACCE *FREE OF CHARGE.*

Contact Teri at intuitgroup@gmail.com or 248.701.8003 for OEM REGISTRATION and SPONSORSHIP info. See our website https://speautomotive.com/acce-conference/ for more information.

THANK YOU TO OUR 2025 ACCE EVENT SPONSORS:

PREMIER PLUS SPONSOR & EXHIBITOR: MP Molding Products

RECEPTION SPONSOR: CSP The Composites Solution Partner

LUNCH SPONSOR: Mitsubishi Chemical Group

PREMIER SPONSORS & EXHIBITORS: ALTA Performance Materials; AOC Trusted Solutions; BASF We create chemistry; Bostik; IDI Composites International; Katcon Global; Westlake Epoxy

ASSOCIATE SPONSORS & EXHIBITORS: Avient; Baylor; Baylor MTACC; Composites One; Century; Covestro; Branson; Emerson; Dickinson Corporation; Dieffenbacher; Fagor Arrasate; fimtec solution; Western; Fraunhofer; IACMI The Composites Institute; Imerys; Kautex; Laval; McClarin; Owens Corning; Rassini; sol epoxy; Toray; Tangho; trimer

ADVERTISING SPONSOR: DSC Consumables Incorporated

MEDIA / ASSOCIATION SPONSORS: Automotive Engineering; AM Additive Manufacturing; CW CompositesWorld; Gardner Business Media, Inc.; Plastics Engineering; Plastics News; Plastics Technology; SAE International; Urethanes Technology

Multifunctional Composites – Self-Health Monitoring Technology

Tymon B. Nieduzak, Luke B. Demo, Maria Q. Feng
Columbia University
Venkat Aitharaju
General Motors

Abstract

This paper presents the development of a multifunctional, self-monitoring fiber-reinforced polymer (FRP) composite battery enclosure for electric vehicles (EVs), capable of detecting both structural damage and lithium-ion battery (LIB) thermal runaway events. Structural carbon fiber tows are leveraged to function as distributed piezoresistive sensors, eliminating the need for additional sensing elements. Measuring the resistance of these structural components enables in-situ monitoring of strain, impact, and fatigue over large areas of the enclosure, offering high spatial resolution and durability without risk of sensor debonding. To enhance thermal runaway safety, micro-temperature sensors are embedded during the molding process. These sensors are lightweight, low-cost, and easily integrated into high-volume manufacturing workflows, where they serve to detect early-stage thermal runaway events, enabling timely response and system shutdown.

Self-monitoring composite specimens are designed, fabricated, and tested to demonstrate efficacy. Resistance changes in the carbon fiber tows during tensile, impact, and cyclic loading conditions are analyzed to enable damage detection, localization, memory, and long-term fatigue monitoring. A machine learning (ML) model trained on this data estimates fatigue life, enabling predictive maintenance and extending the operational life of the enclosure. Thermal experiments and transient finite element heat transfer simulations are used to understand heat propagation through the enclosure when exposed to various thermal runaway conditions. An adaptive ML model compensates for sensor time lag, improving the accuracy of internal surface temperature predictions under dynamic conditions. This integrated sensing platform, which unifies structural, thermal, and predictive health monitoring, advances the design of smart composite enclosures and supports the transition toward safer, more reliable, and scalable electrified transportation systems.

Introduction

As the global automotive industry pivots towards electric vehicles (EVs), the performance, safety, and reliability of lithium-ion battery (LIB) systems have become increasingly critical [1, 2]. While typically very safe, LIBs are susceptible to a catastrophic failure mode called thermal runaway, a condition in which exothermic reactions within the cell lead to uncontrollable temperature escalation. The primary cause of thermal runaway is often a short-circuit fault triggered by separator damage. This damage can result from mechanical impacts, manufacturing defects, electrical abuse, or exposure to extreme

continued on page 9...

This Issue:

AOC
Trusted Solutions

Revolutionize Your Composite Parts with AOC!

Unmatched UV Stability and Durability

Step into the future of SMC formulation technology with AOC. Our groundbreaking solution blends the unparalleled performance of Atryl closed mold resins with Chroma-Tek's high-performing UV stable pigments. This innovative combination sets a new standard for composite pickup beds, tailgates, and other automotive parts, delivering top-tier durability and outdoor performance.

Why Choose Our Composite System?

- Fade-Free: Ultra Black color that resists fading or whitening over time.
- Superior Scratch Resistance: Keeps its sleek black finish, no matter the wear and tear.
- Integrated Color: No need for painting – the color is molded in!

Download the UV Resistant System Whitepaper

Learn more about the formulation and see the outdoor weathering test results.

Atryl CLOSED MOLD FORMULATIONS
Chroma-Tek COLORANTS & ADDITIVES

Leading the Way in Composite Innovation
aocformulations.com/uvresistantsystem

Winning Paper continued...

temperatures [3-11]. Various monitoring and detection systems have been explored, but significant optimization is needed to make thermal runaway detection more effective and commercially viable [12-15].

Among the integral components of EVs, the battery enclosure serves the dual purpose of providing structural support and housing thermal and electrical management systems [16, 17]. However, traditional battery enclosures constructed from steel or aluminum introduce significant weight penalties and are often incompatible with integrated thermal runaway sensing technologies. Consequently, there is growing interest in developing lightweight enclosures from fiber-reinforced polymer (FRP) composites that can simultaneously serve structural, thermal, and sensing functions.

This study introduces a comprehensive, multifunctional composite battery enclosure capable of self-monitoring both structural and thermal states. The innovation stems from three main components: the use of carbon fiber tows as distributed piezoresistive sensors, the integration of micro-temperature sensors embedded during manufacturing, and the implementation of machine learning (ML) algorithms to process sensor data and predict future system behavior. By embedding these capabilities into the composite architecture itself, the resulting system eliminates the need for externally bonded sensors and creates a robust, scalable, and lightweight condition monitoring solution. The primary aim of this paper is to demonstrate the viability of this integrated sensing platform through experimental validation, computational modeling, and data-driven prediction, thereby providing a holistic foundation for the next generation of smart battery enclosures.

Multiple journal and conference papers stemming from this research have been previously published. This article provides a cumulative review and integration of these studies. This summary begins by discussing the structural health monitoring work, detailing the damage detection, localization, memory, and fatigue monitoring along with the fatigue life prediction model using ML. This paper then reviews the temperature monitoring work,

continued on page 10...

detailing the thermal experiments, simulations, and ML temperature inference model. Finally, the implications of an integrated battery enclosure combining these technologies are explained.

Structural Health Monitoring via Piezoresistive Carbon Fiber Tows

The structural sensing capability of the composite enclosure relies on the intrinsic piezoresistive properties of carbon fiber. Carbon fibers exhibit changes in electrical resistance when subjected to mechanical strain, thereby enabling their dual use as both structural reinforcement and distributed sensors. In this work, 3k carbon fiber sensor tows were embedded within a hybrid composite laminate consisting of 19% carbon and 81% glass fiber by volume. The fibers were arranged in a tailored zig-zag stitch pattern across the surface of the composite using customized preform fabrication methods. This configuration enabled widespread monitoring of mechanical strains and damage across the enclosure without introducing additional weight or bonding agents. A novel contact method was developed in this study to

continued on page 11...

DSC CONSUMABLES
incorporated

Est. 2012 Austin, MN

Use the coupon code **SPE** when placing orders online to receive our 20% SPE discount.

www.dscconsumables.com • sales@dscconsumables.com

electrically connect to the sensor tow. The new method, termed silicone over copper (SOC) terminals, was created to enable high volume manufacturing, easily exposing in-molded electrical connections without creating significant stress concentrations. Further details regarding SOC terminals is detailed in the dissertation by Luke Demo [18]. In this investigation, one SOC terminal was installed at each end of the 3k sensor tow, where lead wires were then attached for resistance monitoring. Importantly, the contact points were located outside of the specimens' loaded regions to eliminate variations in the contact resistance during testing.

Structural Damage Detection

The carbon fiber sensor tows were designed in a zig-zag pattern throughout the battery enclosure structure for large-area structural strain monitoring. To validate the efficacy of this design, specimens were fabricated and tested under tensile loads. As shown in Figure 1, the specimens consists of two stacked preforms custom-stitched by Coats Group using tailored fiber placement: (i) a structural preform; and (ii) a sensor preform. (i) The structural preform was made of four unidirectional layers of carbon and glass fiber with in-layer comingled tows. (ii) Adjacent to the structural preform, the sensor preform was made in a custom zig-zag pattern which has been shown to monitor large areas with increased accuracy [19]. Each preform had a glass backing for stitching, which also served as electrical insulation between the sensor and structural carbon fiber tows. Hexion EPIKOTE 06150 epoxy resin and EPIKURE 06150 curing agent were used for the polymer matrix. The specimens were molded and cut following the ASTM D3039 standard specifications [20]. The tensile specimens are shown in Figure 1.

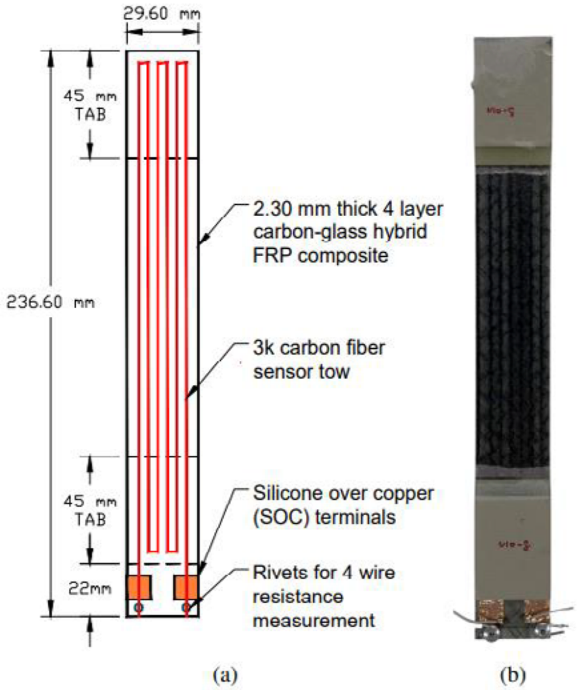

Figure 1: a) Diagram of the fatigue specimen with detailed dimensions, showing the placement of the sensor tow; b) photograph of the fatigue specimen before testing.

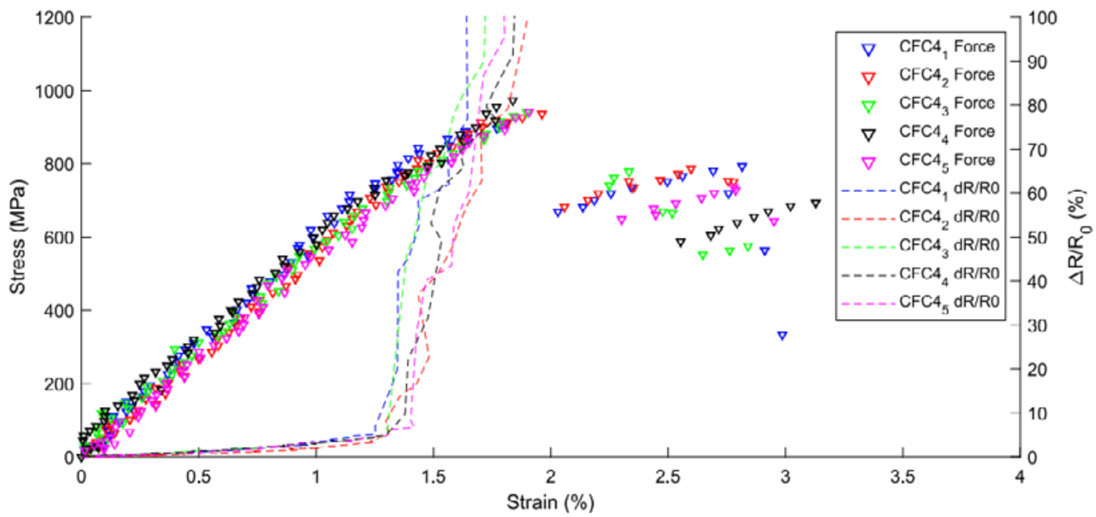

Figure 2: Stress–strain and resistance–strain behavior from tensile testing of hybrid FRP specimens. The carbon fiber sensor tow demonstrates damage detection with a sharp rise in resistance at the first peak of stress, indicating fiber failure.

Five tensile tests were conducted to determine the specimen's ultimate strength. Tests were carried out using an Instron 5984 34k universal testing machine. Each tensile specimen was tested to complete failure, defined as a 70% reduction in the relative load. The tests were performed under displacement control with a crosshead speed of 1.0 mm/min, as suggested by ASTM D3039 [20]. The tensile test results, shown in Figure 2, revealed the characteristic M-shaped stress-strain response typical of hybrid carbon-glass fiber composites. This response featured two distinct failure peaks corresponding to the sequential rupture of carbon and glass fibers. The embedded carbon fiber sensor tow exhibited a nearly linear resistance response up to approximately 1.25% strain, after which a nonlinear, asymptotic rise in resistance signaled the onset of progressive carbon fiber breakage. The resistance approaches infinity prior to catastrophic failure of the glass fibers, highlighting the piezoresistive sensor's capability to detect early-stage damage.

continued on page 13...

Structural Damage Localization

An alternative design of the sensor tow layout was developed to enable structural damage localization across a large area. This innovative design connects carbon fiber sensor tow branches in parallel to one pair of sensor terminals, thus significantly saving manufacturing costs. By carefully designing the resistance values of each sensor tow branch, the location of damage in a specific sensor tow can be inferred using the change in the overall circuit resistance [21]. The efficacy of this low-cost damage detection and localization method was experimentally validated through impact tests. These impact tests evaluated the system's ability to detect and localize impact structural damage, simulating real-world events such as road debris strikes or crash scenarios. These studies involved high-velocity impact testing on large composite panels embedded with carbon fiber sensor tows looped in different orientations. The fabrication followed similar steps as the tensile specimens, but the sensor tow layout was modified. The innovative multi-branch design, as shown in Figure 3a, facilitates damage localization within a large area using only one pair of sensor terminals that minimize manufacturing burden and cost – See [21] for more details. A calibrated drop-weight impactor was used to generate controlled damage at predefined locations, while the distributed sensing network recorded resistance changes in real time, illustrated in Figure 3b.

For the damage localization system to distinguish failure between the various carbon fiber circuit branches, each branch must have a unique resistance, intrinsically produced by carbon fiber tows of differing lengths (and potentially further modified using additional in-line resistors which improve the damage detection resolution). Once the number of branches required to monitor the desired panel area is determined, it is possible to establish the circuit equivalent resistance and the expected changes in that value caused by different damage scenarios. The damage localization algorithm determines the equivalent resistance of the circuit when all the branches are intact, reads the updated resistance, and determines whether the updated resistance falls within the

continued on page 14...

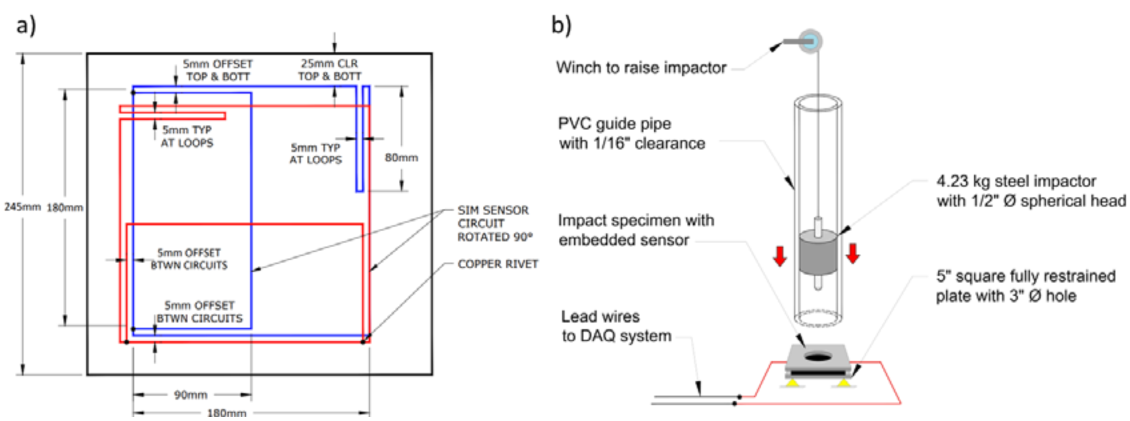

Figure 3: a) Impact specimen design with orthogonal red and blue carbon fiber damage localization circuits; b) Impact experimental setup.

This Issue:

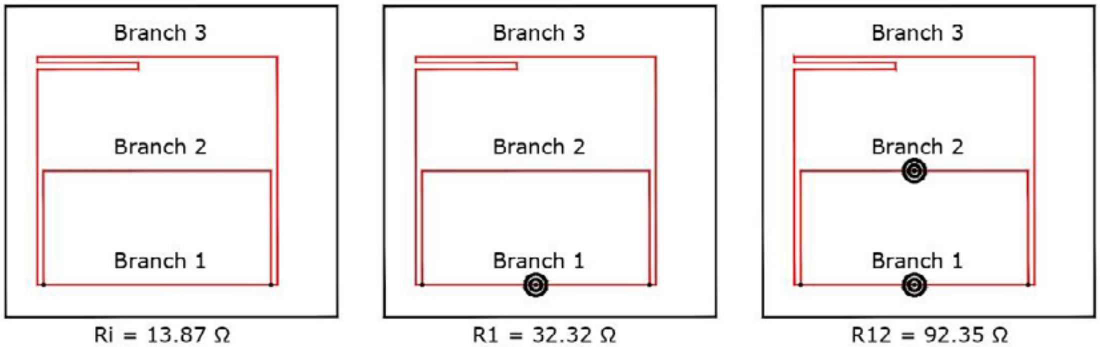

Figure 4: Equivalent resistance of the red three-branch circuit due to various damage scenarios. A ruptured branch, with resistance approaching infinity, is denoted with a bullseye.

range of the equivalent resistance associated with the undamaged circuit. If the measured resistance falls outside this range, the circuit is considered damaged, and then the methodology looks for the correct identification of the damage. With this correspondence, the damage scenario is determined as each outcome corresponds to a unique failure scenario. The metrics error (ε), margin of error (μ), and error utilization (ϕ) are introduced to qualify the identification accuracy. The error is determined as the difference between the predicted damage scenario resistance and the measured resistance. The aforementioned metrics can be calculated as absolute values or percentages. Finally, error utilization (ϕ) is the ratio of the error to the margin of error. Good identifications can be parsed from poor identifications as a low error utilization denotes a successful damage identification. The calculations and methodology are further explained in the study by Demo et al. [21].

The impact locations for three of the seven damage scenarios are shown in Figure 4. The drop tower was set with an impactor height that consistently broke the targeted sensor tow. Ri (13.87 Ω) represents the starting resistance value of the undamaged three-branch circuit, R1 (32.32 Ω) represents the first branch breaking with the second and third branches intact, R12 (92.35 Ω) represents the first and second branch breaking with the third intact and so on.

continued on page 15...

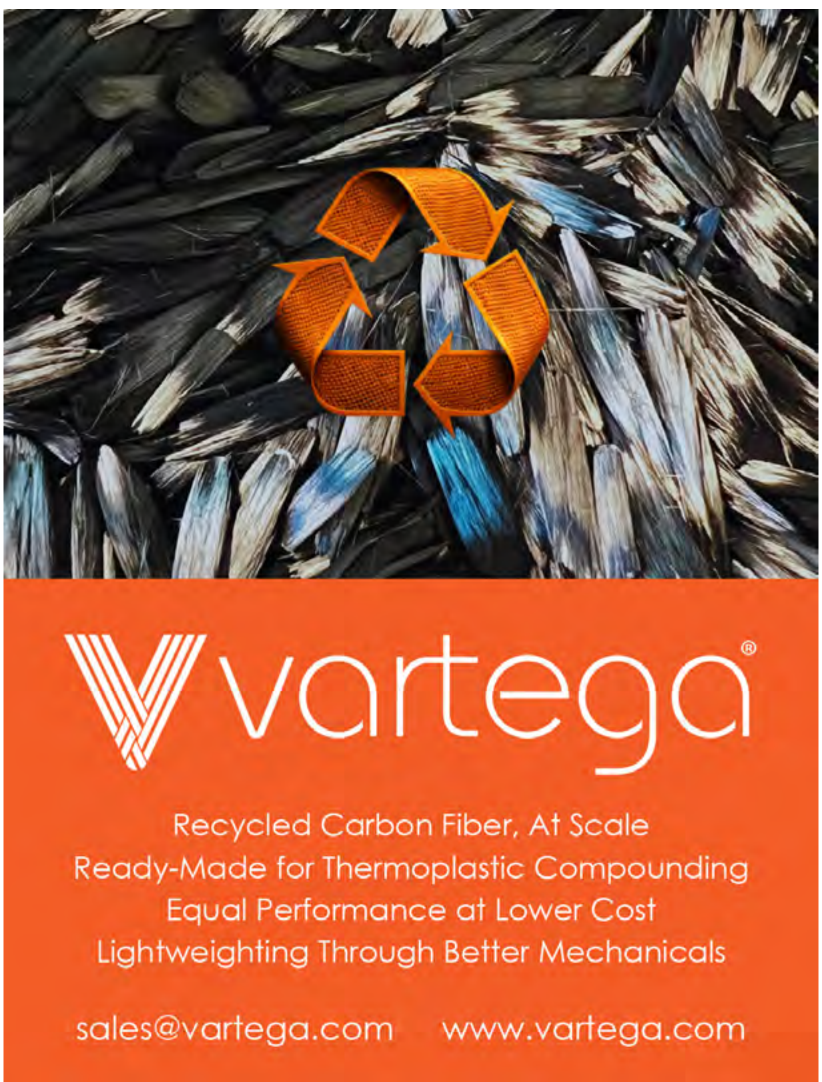

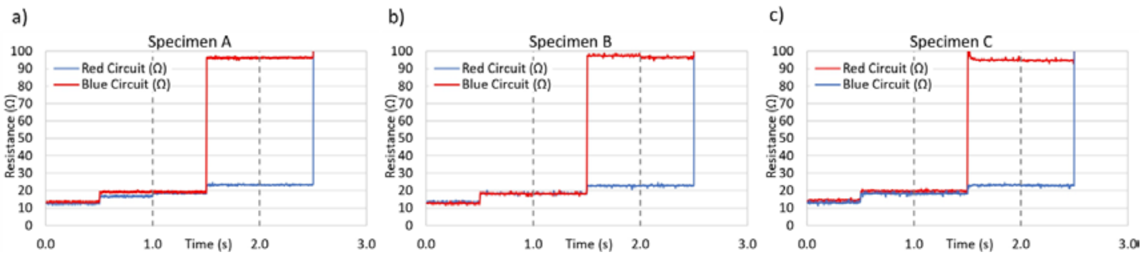

Figure 5: Impact test resistance versus time, showing three impacts spliced back-to-back: Impact 1 spans 0–1 s, Impact 2 spans 1–2 s, and Impact 3 spans 2–3 s.

To test the adequacy of the sensor, a three-impact sequence was selected to target the system's more challenging identification scenarios. The first impact was near branch 2 of both red and blue sensors (damage scenario R2). The second impact was near branch 3 of the red circuit (damage scenario R23) and branch 1 of the blue circuit (damage scenario R12). Finally, the third impact (damage scenario R123) was near the last remaining branch of each circuit: branch 1 of the blue circuit and branch 3 of the red circuit. Resistance versus time was monitored during the impact and is shown in Figure 5. The three impact recordings were spliced back-to-back and combined into one figure.

In Figure 5, the first impact spans the 0 s and 1 s window, with the impact centered at 0.5 s. Similarly, the second impact spans between 1 s and 2 s, while the third and final impact is between 2 s to 3 s. The measured resistances demonstrate a high degree of correlation to the predicted values, indicating that the damage localization system has the ability to correctly identify the damaged branch. For example, in Specimen A, the first impact damaged branch 2 of the blue circuit, changing the equivalent resistance from 13.96 Ω to 19.05 Ω. Using the new resistance value, the location can be identified with high confidence, as the 19.05 Ω resistance was near the center of the 19.23 Ω identification bucket with boundary values of 17.77 Ω and 21.76 Ω. In this case, the absolute measurement error is 0.18 Ω and the relative error is 0.96%. Similar error analysis can be applied to all the impact tests, finding a mean absolute error of 0.54 Ω with a standard deviation 0.55 Ω, and a mean relative error of 2.95% with a standard deviation 2.20%. Impact 3, which resulted in near-infinite resistance, was not used in the mean error analysis, as it would have misleadingly reduced the mean error. The sharp increases in resistances were confined to the affected regions, while unaffected regions showed negligible changes. The minimal error in the correlation between measured resistance values and predicted damage scenarios affirms the system's capability to accurately identify and localize damage in FRP composites.

Structural Damage Memory

As revealed in the damage detection tensile tests shown previously, when the specimen strain increased to the linear-nonlinear transition value, some sensing carbon fiber filaments started to break, resulting in a drastic and irreversible increase in overall resistance. To further investigate this phenomenon and explore this permanent resistance increase as damage memory, impact tests were conducted using the same drop-weight impactor setup as the

continued on page 16...

This Issue:

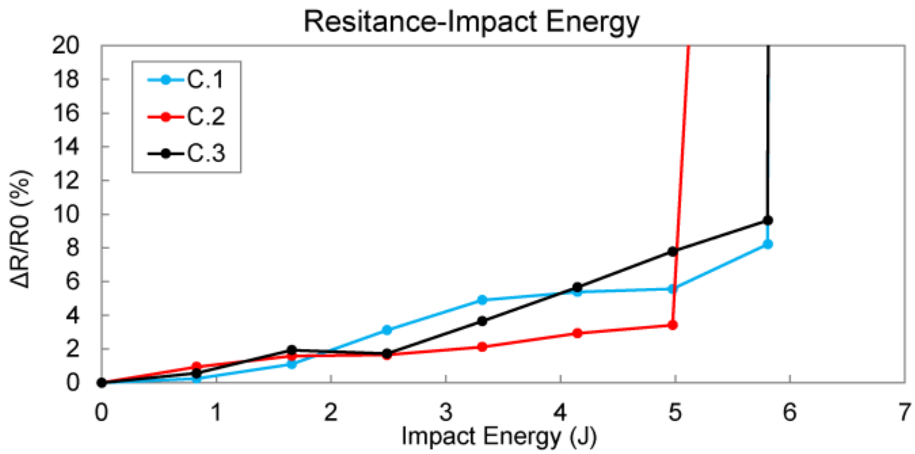

Figure 6: Permanent change in resistance of 3 identical impact specimens with increasing impact energy.

previous section. These impact tests did not immediately break the targeted sensor tows, but progressively increased the impact load, specifically exploring lower impact energies. In total, three identical single sensor specimens were built and tested (C.1, C.2, and C.3), and each was subjected to seven impact tests with progressively increased impactor heights. The first test was conducted with a drop height of 2 cm, which corresponds to an impact energy of 0.85 J. Each subsequent test was 2 cm higher than the previous test. Testing was concluded once the specimens reached total failure and the sensor resistance approached infinity.

Figure 6 plots the post-impact resistance values (percent change versus the initial pre-experiment resistance) as a function of impact energy for the three tested specimens. All three specimens show a nearly linear relationship between impact energy and permanent change in resistance before complete failure. Specimens C.1 and C.3 failed after the seventh impact at 5.8 J, and the resistance concurrently approached infinity. Specimen C.2 saw a large increase in the resistance value after the sixth impact at 4.97 J before similarly failing afterward.

The progressive impact tests demonstrate the intrinsic damage memory and early-warning functionality of the carbon fiber sensor tow – the specimen's impact history is captured by the sensor tow's resistance values. Each time the specimen suffered impact damage, the resistance increased, which was irreversible, demonstrating that resistance can be used as the primary variable for damage early warning. As shown by Li et al. [22] and Kalashnyk et al. [23], the change in resistance can be expressed as a function of discontinuous filament paths, and accordingly, the proportion of damaged fibers can be extrapolated. This correlation between electrical resistance and intact fibers gives a continuous, in situ assessment of overall composite health. These findings confirm that the embedded carbon fiber sensors are capable not only of detecting and locating damage, but also remembering damage as it accumulates, which is crucial for targeted inspection and repair in practical EV applications.

continued on page 17...

This Issue:

ACCE Award Winning Paper continued...

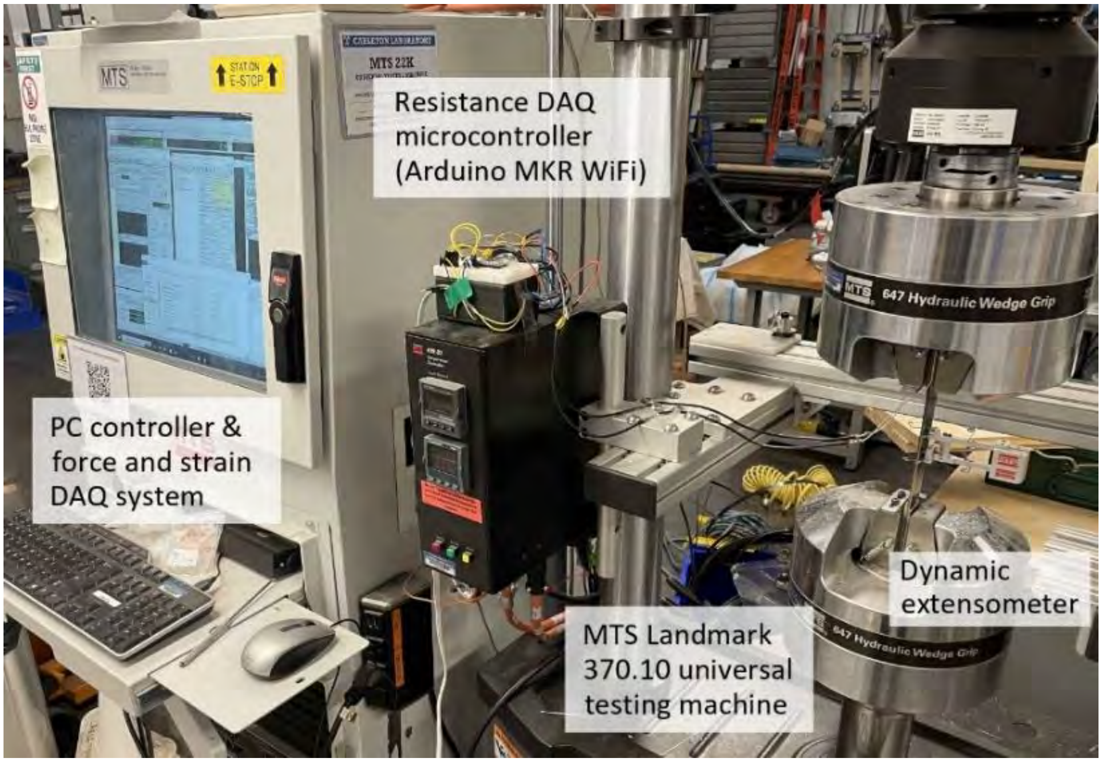

Figure 7: Fatigue test setup showing the DAQ systems for force, resistance, and strain.

Fatigue Damage Monitoring

The capability of self-sensing carbon fiber sensors in monitoring structural fatigue was further investigated. Fatigue tests were conducted using an MTS Landmark 370.10 universal testing machine under load-control. Actuator force command and actuator force response were recorded using the onboard MTS universal testing machine load cell and DAQ. Strain was measured with an MTS dynamic extensometer, model number 634.12E-24, which also connected to the onboard MTS universal testing machine DAQ. Both systems were set to a write-to-file sampling rate of 256 Hz. Resistance was monitored using a custom-built Arduino MKR WiFi 1010 microcontroller which measures resistance at a sampling rate of 256 Hz using a voltage divider circuit. The fatigue test setup is shown in Figure 7.

Fatigue testing was performed on thirteen specimens under tension-tension loading across five different normalized stress levels ranging from 45% to 80% of the material's ultimate tensile strength. The fatigue specimens were fabricated identically to the tensile test specimens described earlier. In Figure 8, one representative specimen is shown for four of the five stress levels (42.5%, 60%, 70%, and 80%), illustrating the most significant variations in measurements.

The observed trends in resistance response were consistent across stress levels. At lower stress levels, resistance remained relatively stable for over 100,000 cycles, indicating minimal progressive damage. As the applied stress increased, the resistance began to rise gradually with cycling,

continued on page 18...

This Issue:

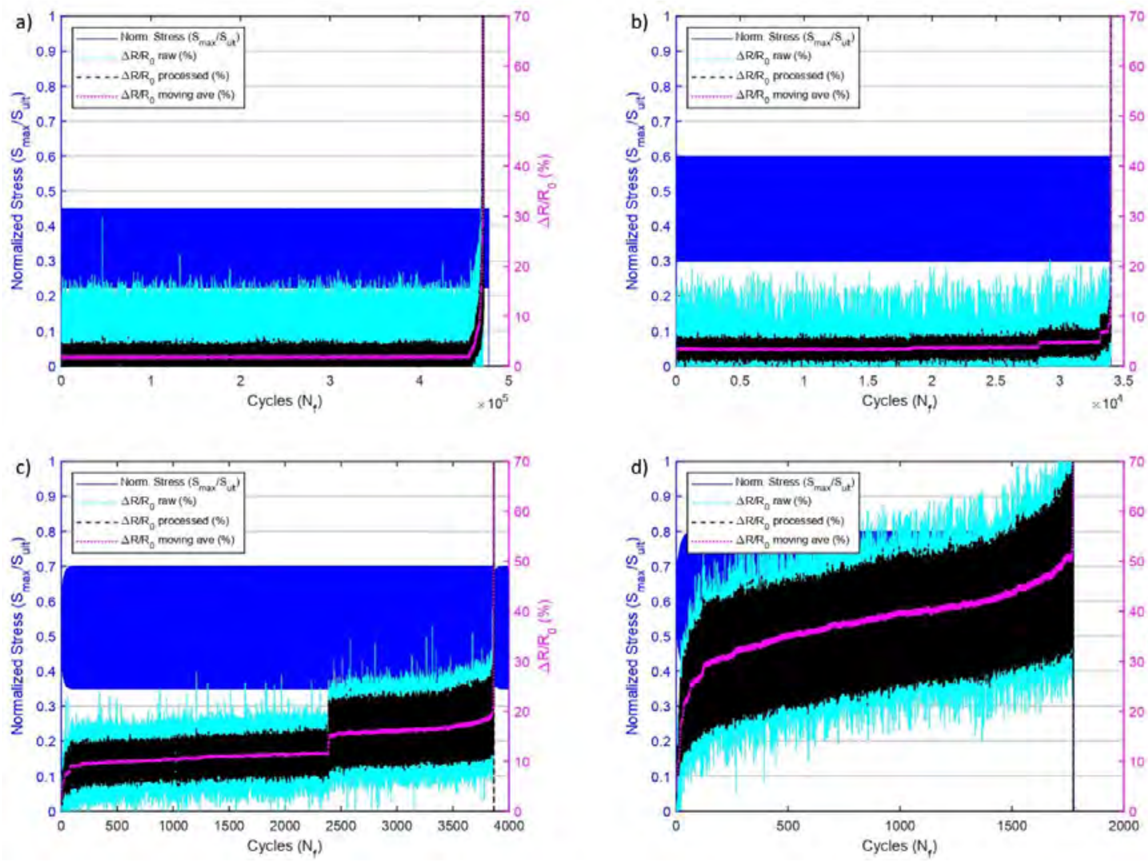

Figure 8: Fatigue test results showing the resistance and stress profiles over time for different stress levels applied to specimens a) 42.5%, b) 60%, c) 70%, d) 80%. The resistance increases sharply before failure, indicating sensor effectiveness for damage early warning.

and eventually increased nonlinearly, in tandem with damage accumulation. At the highest stress levels, specimens failed within a few thousand cycles, with resistance signals providing clear precursors to failure. In several cases, a sharp resistance spike occurred within the final 2% to 10% of the specimen's fatigue life, offering a reliable early warning of imminent structural failure. These results confirm that the embedded carbon fiber tow is capable of long-term, real-time monitoring of fatigue damage with high sensitivity.

Machine Learning Fatigue Life Prediction Model

While raw resistance data provides valuable information about the material state, its full potential for predicting fatigue life is unlocked through the use of data-driven ML predictive models. A long short-term memory (LSTM) neural network was employed to analyze time-series resistance data from the fatigue experiments and predict the remaining useful life (RUL) of the specimens. The LSTM architecture was chosen for its ability to model temporal dependencies and capture both transient and cumulative damage signatures present in the resistance signal. The

continued on page 19...

This Issue:

ACCE Award Winning Paper continued...

architecture applied in this work consists of a sequence input layer, followed by an LSTM layer with 150 hidden units. This structure allows the model to capture information on both past and future states. The LSTM layer is governed by three gating mechanisms: the input gate, the forget gate, and the output gate. These gates control the flow of information through the cell state and hidden state. This allows the network to decide what information to keep and discard. The update equations utilize the sigmoid activation function, and the sequence of gates collectively determine the updated cell state.

To train the model, resistance data was preprocessed to extract five key features that reflect both short-term fluctuations and long-term degradation. These included moving window statistics (mean, max, and min), moving amplitude of resistance, time-integrated resistance (representing cumulative damage energy), a cycle-based feature derived from rainflow counting methods, and a combined feature created by dividing the integrated resistance by the log-normal rainflow cycles. More explicit details of the model architecture and feature engineering can be found in the study by Demo et al. [24]. Combining all five features enables the model to learn the short-term oscillatory behavior and the long-term accumulative fatigue damage. The network was trained on data from all thirteen fatigue specimens, with careful alignment and down-sampling of the signals to accommodate computational constraints.

continued on page 20...

Sponsor the Newsletter

Quarter page ad or logo ad:
3.75" x 5" $500

Half page ad:
7.5" x 5.5", 5" x 7.5", 4" x 8.5"..................$750

Full page ad:
7" x 10", 8.5" x 11" $1,250

Contact: Teri Chouinard CBC, APR
SPE Composites Division
Sponsorship Chair
C/O Intuit Group, Inc.
phone 248.701.8003
intuitgroup@gmail.com

Please provide Logos as JPG and EPS files
(send both if possible)
Please provide Ads as High Resolution PDF files
Advertising with the SPE Composites Division is inexpensive and easy. Please help us to promote the benefits of Composites in Industry.

Sponsoring the Newsletter enables the SPE to communicate the benefits of the composites in many industries, which fortifies your marketing efforts.

- **Support your SPE Composites Division**
- **Reach 1,000 Composites Professionals 3 Times a year via the E-Newsletter**
- **Also reach 1,070 SPE Composites Division Linked In Members 3 times a year and an additional 11,492 COMPOSITES Linked In Members Secondary group where the link to the newsletter is posted year-round**
- **Reach many more as a sponsorship also includes your logo on our website, www.composites.4speorg with a link to your company**
- **Maximize your exposure to the customers & the trade**
- **Stay informed on the latest composites activity**

Increase your presence on the web leading to more sales by sponsoring our Electronic Newsletter which is published on the SPE Composites Division Website and emailed to all Division Members (1,000 approx.) 3 times annually. Rates include 3 issues (not on calendar basis - published approx. Nov/Dec, Mar/April, July/August). All ads include a link to your website increasing your exposure on the worldwide web exponentially. Sponsorship also includes your logo ad with a link to your website on www.composites.4speorg further increasing your presence on the Web as a Leader in Composites Technology.

This Issue:

In each prediction, the LSTM neural network produces a temporally varying sequence and models both the short-term and long-term temporal dependencies. Each sequence is fed into a dropout layer with a dropout rate of 0.3, preventing overfitting by randomly eliminating 30% of neurons during training. After, a fully connected layer follows, containing L2 regularization with a weight decay factor of 0.001. The L2 regularization aids in generalization by penalizing large weights. In order to effectively train the model, the adaptive learning rate optimizer Adam was used, which modifies the learning rates based on the first and second moments of gradients. To facilitate model convergence, an initial learning rate of 0.002 was used with a scheduled decrease by a factor of 0.2 after 50 epochs. The model was trained for 200 epochs with a mini-batch size of 128. Error was minimized based on the mean absolute error (MAE) criteria. MAE was selected over root-mean-square error due to its improved capacity for outlier tolerance, which were not uncommon in the noisy resistance dataset. The target remaining life used for training is defined as the complement of cumulative damage. The target remaining fatigue life helps evaluate the general accuracy of the prediction model but does not represent the exact ground truth. Further explanations of the ML parameters and target remaining life calculations are included in the study by Demo et al. [24].

continued on page 21...

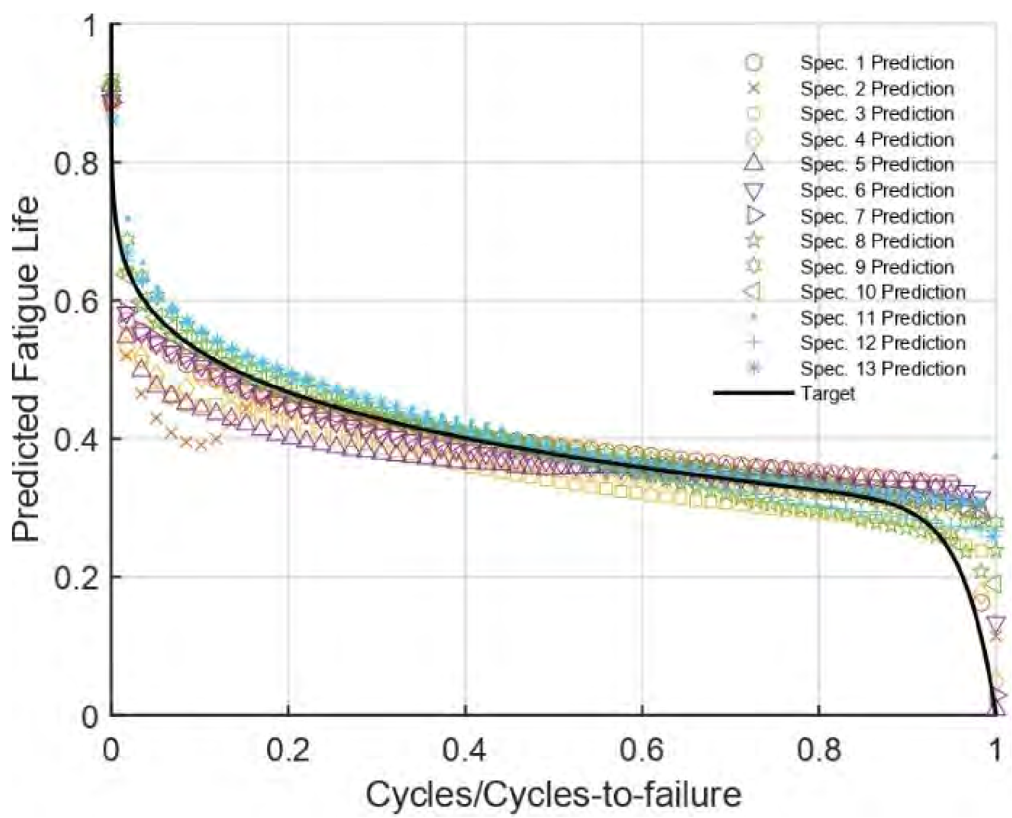

Figure 9: Fatigue life prediction using the LSTM neural network for 13 specimens. The black line represents the target remaining fatigue life.

This Issue:

ACCE Award Winning Paper continued...

To validate the prediction model, a k-fold analysis with five folds was implemented. In a k-fold analysis, data is divided into multiple subsets, where the majority of the data is used for training, and the remaining data is used for testing. For the 13 fatigue testing datasets, between 10 and 11 specimens were used for training, and the remaining two or three were used for evaluation. Figure 9 shows the LSTM neural network fatigue life prediction results for all 13 specimens, and the black line represents the target fatigue life remaining.

The resulting model demonstrated excellent predictive performance, achieving high R2 values and low MAE, indicating the model's robustness across varying loading conditions. Predictions of cycles-to-failure for held-out validation sets showed errors consistently below 7%, with only one outlier (specimen 2) reaching an error around 10%. This specimen was tested at the lowest stress level, revealing that it becomes more difficult to extract signal features when the resistance does not demonstrate a clear trend throughout the duration of the test. However, this disparity may be a feature of the damage progression rather than an error, the difference reflecting the specimen's unique internal mechanics with the predicted values being a better indicator of true remaining life. Importantly, the model achieved these results without requiring stress or strain inputs, relying solely on resistance data, thereby simplifying sensor instrumentation and broadening the applicability of the system to a variety of deployment scenarios. This study demonstrated the effectiveness of a self-sensing carbon fiber tow powered by neural networks for real-time fatigue life prediction in the composites.

Thermal Monitoring via Embedded Micro-Sensors

In addition to structural integrity, thermal safety is a paramount concern in LIB systems, particularly due to the risk of thermal runaway. To address this, STS4x digital micro-temperature sensors were implemented to monitor temperature changes [25]. FRP composites facilitate sensor embedment in sublayers through a one-step molding process, removing the need for extra surface mounting steps or adhesives. Embedding the sensors also addresses the tight space constraints of this application and offers sensor protection. Despite these benefits, sensor embedment introduces challenges, including a time lag in detecting internal surface temperature. Since a layer of composite separates the embedded sensor from the surface, a time lag in temperature detection occurs as heat flows through this overlaid composite layer. Characterizing and addressing this time delay is crucial for an effective thermal runaway early warning system within the enclosure.

A prototype test sample representing a portion of a LIB enclosure was developed to explore the thermodynamic properties of a hybrid FRP composite instrumented with micro-temperature sensors. The sample, a carbon and glass FRP composite measuring 180 mm by 300 mm, resembled a section of a LIB enclosure underneath a single battery module. It comprised 4 layers of 81%/19% glass-to-carbon material in a 0/90/90/0 orientation. The micro-temperature sensors, measuring 1.5 by 1.5 by 0.5 mm, were embedded into the composite structure during fabrication using the same preform placement techniques employed for the carbon fiber sensor tow.

continued on page 22...

This Issue:

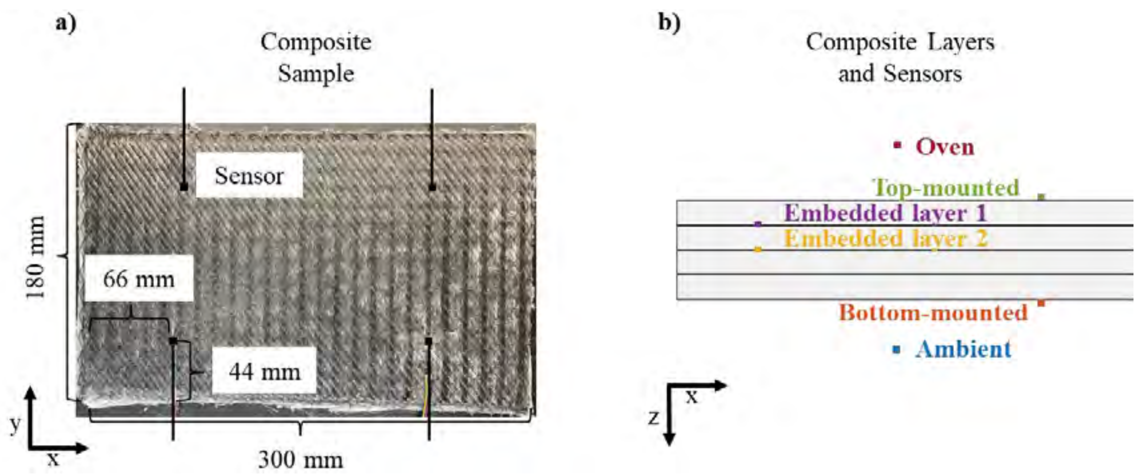

Figure 10: a) Overhead view of the composite sample showing the locations of the temperature sensors in the x-y plane along with the total sample dimensions; b) Cross-sectional view of the composite layers illustrating the placement of the temperature sensors in the z-direction along with the external oven and ambient sensors.

The embedded sensors were strategically placed at four locations within the composite specimen: two on the surfaces (top and bottom) and two within the inner layers (layer 1 and layer 2). All four sensors were used to inform and verify the finite element heat transfer simulation discussed below. The top surface mounted sensor and embedded layer 1 sensor were specifically utilized in the following ML study. The goal was to investigate the thermal response time of embedded sensors relative to surface-mounted versions under conditions mimicking real-world thermal runaway events. Physical thermal experiments were conducted using a modified lab oven, replicating various early thermal runaway propagation conditions. Two more sensors measured the environmental temperatures above and below the top and bottom surfaces (oven and ambient). The sensor placements are shown in Figure 10.

Experimental Replication of Thermal Runaway Conditions

Two types of thermal experiments were conducted representing different thermal runaway mechanisms: thermal shock tests in which the instrumented enclosure sample was rapidly exposed to high oven temperatures, and thermal ramp-up tests where the temperature was increased gradually to simulate slower heating scenarios. During LIB thermal runaway, heat transfer occurs unidirectionally through the enclosure due to the high-temperature battery failure on the top surface and ambient conditions on the bottom surface. To simulate this, a novel experimental setup involving a lab oven sealed with an expanded polystyrene foam (EPS) sheet was devised. The composite sample was sealed into a void in the middle of the EPS sheet, which covered the oven opening. This setup exposed the sample's top face to oven chamber conditions (representing battery enclosure internal temperatures) while the bottom face was exposed to ambient room temperature. Figure 11 presents a diagram of the experimental setup.

continued on page 23...

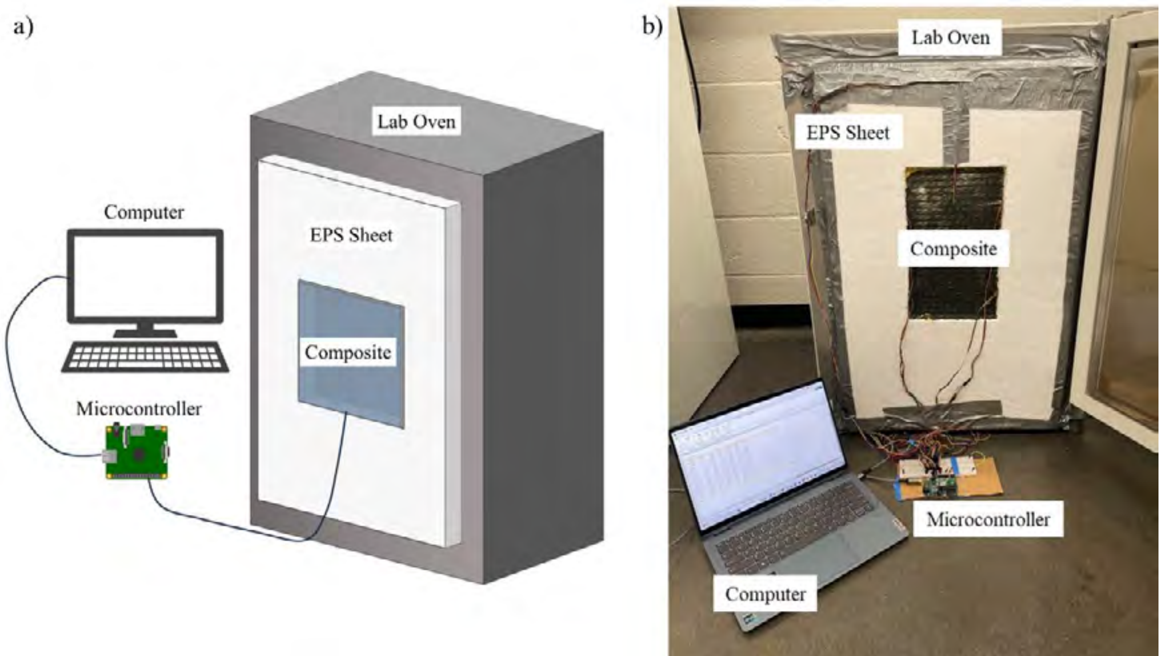

Figure 11: Experimental setup detailing the composite, the EPS sheet 'oven door', the lab oven, the microcontroller, and the computer. a) Experimental setup diagram; b) Experimental setup picture.

Four maximum temperatures were imposed for both the thermal shock and ramp-up scenarios (120°C, 100°C, 80°C, and 60°C), and the experiments were replicated three times at each condition to validate the consistency of the measurements. These tests generated a total of 24 experimental composite thermal response datasets.

Finite Element Heat Transfer Simulation

To further characterize the temperature sensing time delay, a three-dimensional transient heat transfer model was developed using the OptiStruct finite element solver. The composite was modeled at the meso-scale, incorporating detailed geometry of carbon and glass fiber tows embedded in an epoxy matrix. Material properties for the composite components were projected from literature sources and discussions with suppliers, then calibrated to closely align with the experimental temperature curves obtained from the initial 120°C thermal shock test [26, 27]. Anisotropic thermal conduction coefficients were specifically applied to the carbon fiber tows to account for the fibers' higher axial conductivity compared to radial. Experimental temperature curves from both the oven and ambient sensors were imposed as convective thermal loads on the simulated composite sample's top and bottom surfaces. The forced convective heat transfer coefficients for the top and bottom surfaces were adjusted based on theoretical assumptions and experimental findings. Three finite element simulations were conducted for each temperature condition, utilizing the experimental ambient and oven temperatures from each repetition as input thermal loads, generating a total of 24 simulated composite thermal response datasets. Additional details regarding the finite element simulation parameters can be found in the study by Nieduzak et al. [28].

continued on page 24...

This Issue:

ACCE Award Winning Paper continued...

Temperature trends from both the experiments and simulations for each repetition of the thermal shock tests at 120°C, 100°C, 80°C, and 60°C are illustrated in Figure 12. The oven and ambient temperatures (environmental conditions) are outlined in Figure 12a, while the thermal response of the composite, including the top, layer 1, layer 2, and bottom temperatures, are shown in Figure 12b. The variation observed across the three repetitions of each test is shown by shaded error bars around each curve. These error bars denote the standard deviation derived from the repetitions, with the mean results of the tests depicted as lines. Within the finite element model, the locations of the sensors were pinpointed, and corresponding nodes were selected to extract equivalent datasets from the simulations. The simulated results are depicted as dashed lines while the experimental

continued on page 25...

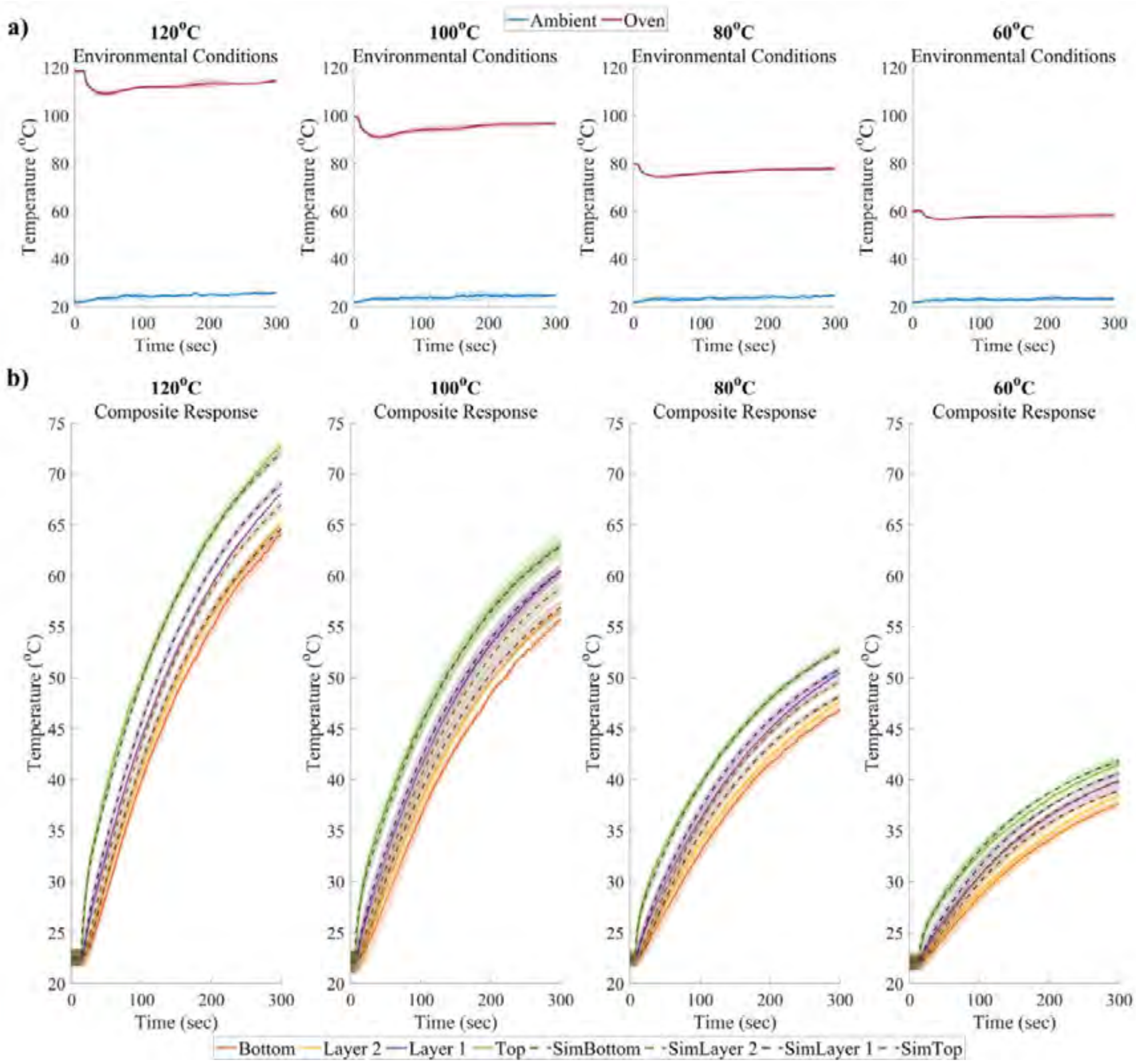

Figure 12: Thermal shock experimental and simulation results for each repetition at 120°C, 100°C, 80°C, and 60°C. a) Oven and ambient environmental temperature curves; b) Composite response temperature curves.

This Issue:

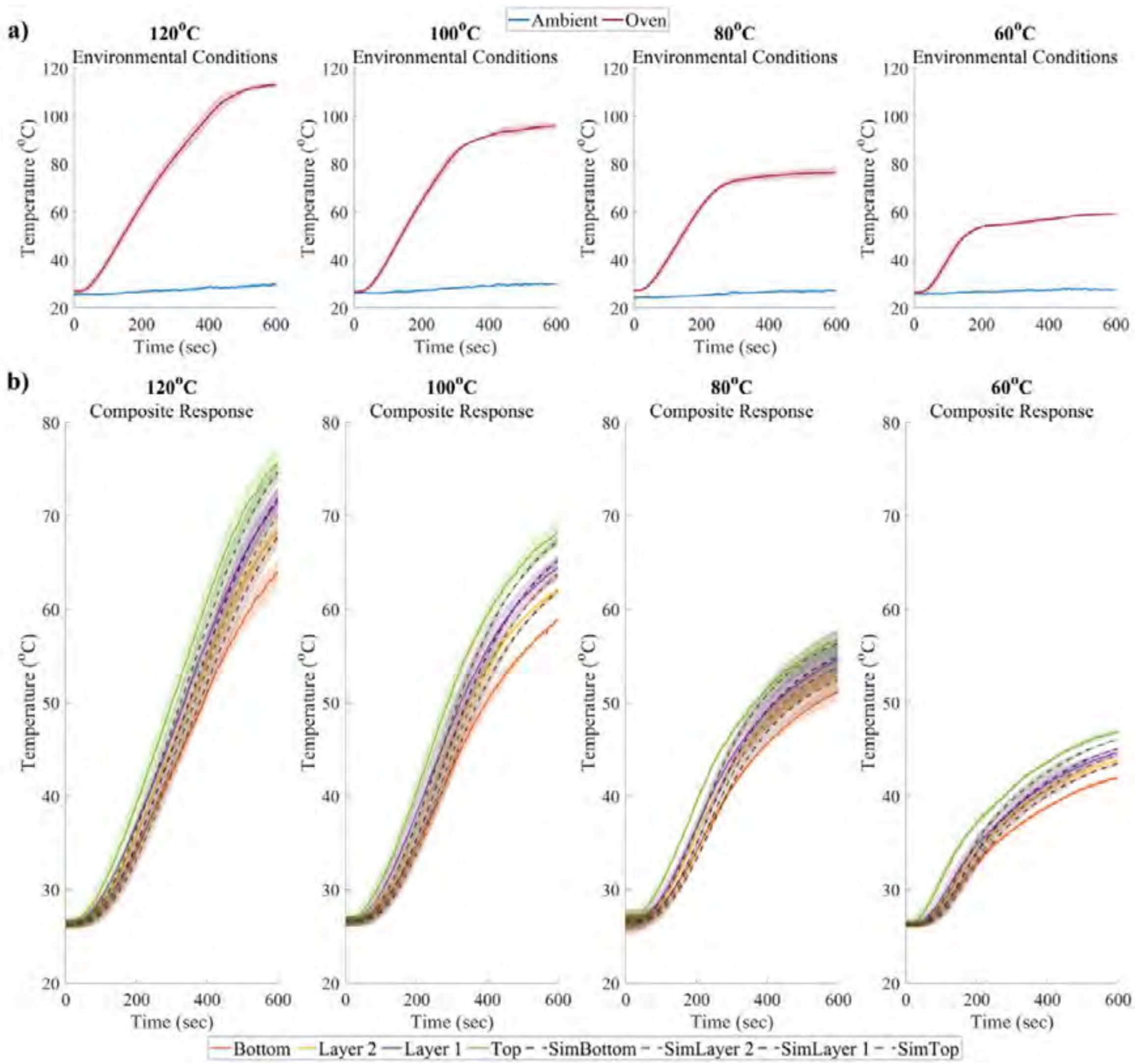

Figure 13: Thermal ramp-up experimental and simulation results for each repetition at 120°C, 100°C, 80°C, and 60°C. a) Oven and ambient environmental temperature curves; b) Composite response temperature curves.

curves are shown as solid lines. Figure 13 presents the results for the thermal ramp-up experiments and simulations in the same manner as Figure 12.

The errors in the heat transfer simulations with respect to the experimental results were quantified using mean absolute percentage error (MAPE) for both the thermal shock and thermal ramp-up datasets. The MAPE values between the simulations and experiments were maintained below 0.065%, revealing the high accuracy of the thermal model projections. These results support that the composite's thermal response can be accurately estimated by the tuned simulation if other realistic thermal runaway conditions were imposed.

continued on page 26...

This Issue:

Machine Learning Temperature Inference Model

Building on the experimental results and validated finite element simulations, a ML model was developed to infer actual internal surface temperatures from embedded sensor readings experiencing the time delay. It is not possible to use a simple analytical, bilinear, or piecewise function to represent this relationship as these approaches are not representative of the heat transfer intricacies induced by different thermal runaway mechanisms. Therefore, an adaptive ML approach is implemented for this application as the relationship between the surface temperature and embedded layer measurement depends on the imposed temperature condition.

A substantial dataset of composite thermal responses is necessary to train and test a generalized ML model. A flowchart detailing the input dataset sources and data processing is shown in Figure 14. This dataset was founded on the experimental and simulation results of the prior work (a total of 48 thermal responses) and augmented with an additional 24 simulations, imposing thermal shock and ramp-up thermal loads with added noise. The added noise introduced variability in the thermal responses, increasing the dataset dimension and improving the ML algorithms' generalization. Next, a set of more realistic thermal runaway temperature curves were generated and imposed in the simulation, based on experimental measurements of real LIB thermal runaway events in the literature [29]. These representative temperature curves derived from literature were implemented in the model as thermal loads. These simulated composite responses to more realistic thermal runaway conditions were extracted and used in the ML algorithms' testing set, noted as 'realistic thermal simulations' in Figure 14.

continued on page 27...

This Issue:

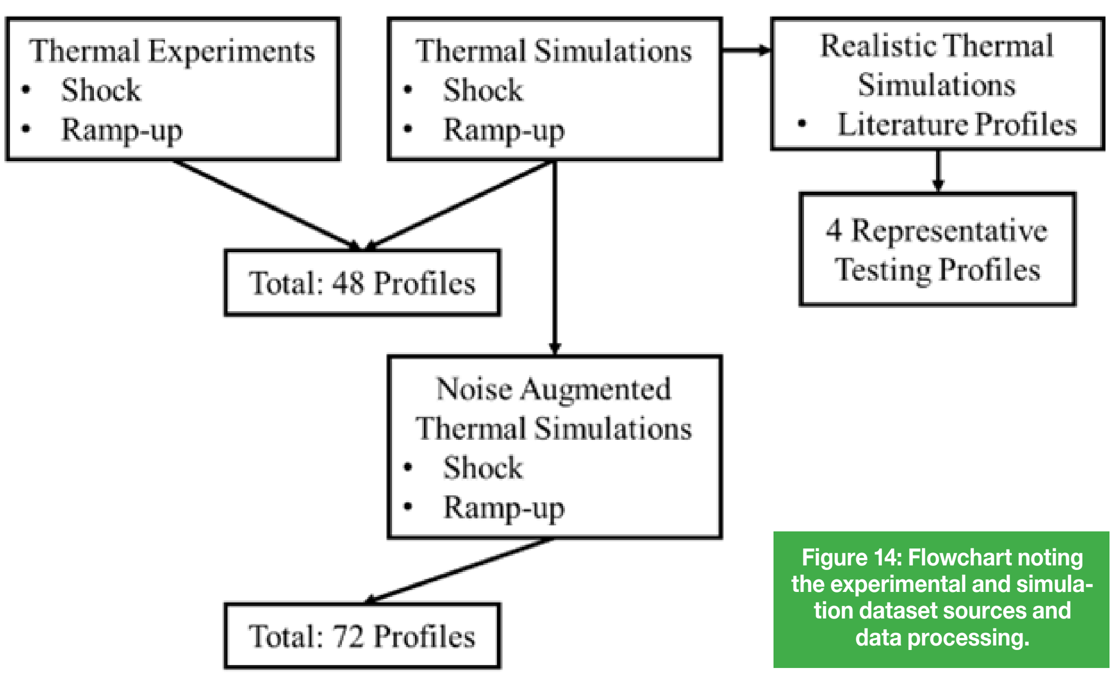

Figure 14: Flowchart noting the experimental and simulation dataset sources and data processing.

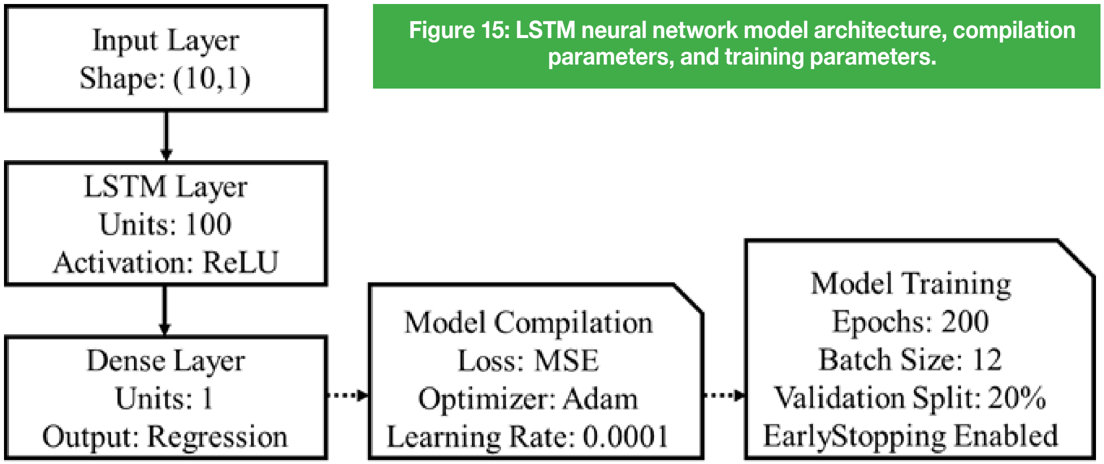

Figure 15: LSTM neural network model architecture, compilation parameters, and training parameters.

This configuration formed a supervised ML regression framework, wherein the temperature data from embedded layer 1 served as the input feature, and the data from the surface acted as the target output. By training on paired embedded and surface sensor data, the model learned to correct for the time lag and provide real-time temperature estimates of the enclosure's interior surface. During the model training process, a strategy of randomly selecting data points from each dataset was employed for validation purposes, enabling evaluation of the model's performance through the assessment of validation loss using mean squared error (MSE). Additionally, the four realistic thermal simulation results implementing thermal runaway profiles from literature were reserved for a representative testing phase, assessing the model's performance when the composite is exposed to varying conditions more closely approximating those that precede a real thermal runaway event.

Several models were tested, the highest performance achieved by an LSTM neural network. This model employed the rectified linear unit (ReLU) as the activation function, renowned for its effectiveness in avoiding the vanishing gradient issue. Adaptive moment estimation (Adam) was the optimization algorithm utilized, chosen for its efficiency in updating network weights and handling sparse gradients [30]. During model exploration, emphasis was placed on a streamlined neural network architecture. Specifically, only one hidden LSTM layer was to be incorporated, leveraging the TensorFlow Keras library. The model's architecture, compilation parameters, and training parameters are depicted in Figure 15.

The input consists of a one-dimensional sequence that captures the temporal dynamics within a sliding window of size 10. This design choice facilitated the processing of time series data, allowing the model to effectively learn from sequences of past data points to predict future values. The architecture implements a single hidden LSTM layer equipped with 100 units, providing a substantial capacity to capture the temporal dependencies in the data. The culmination of this architecture is a final dense layer consisting of a single neuron, reflecting the objective to predict a single internal surface temperature data

continued on page 28...

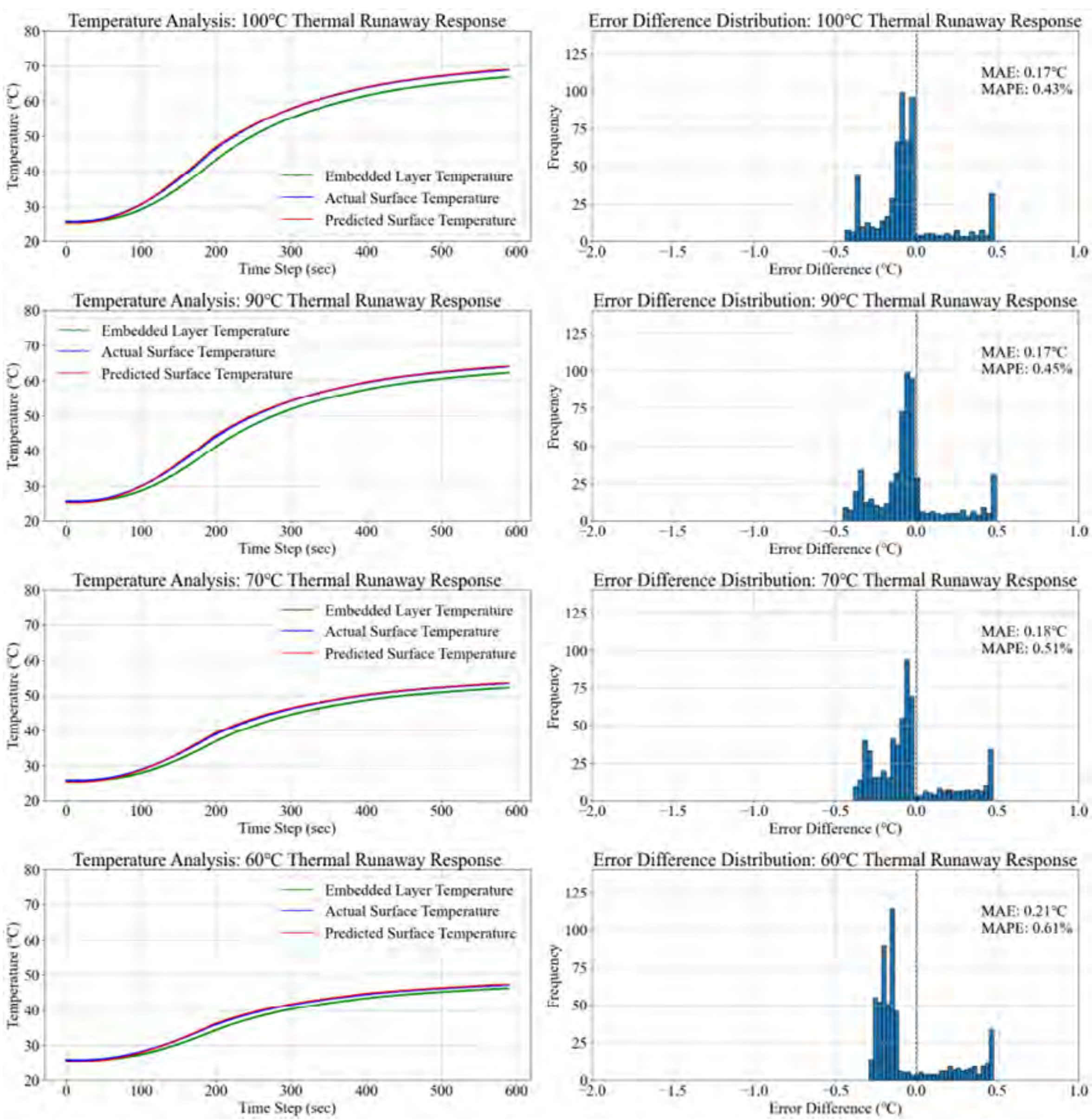

Figure 16: LSTM neural network validation assessment results.

point at each time step. This structure was chosen to balance the model's ability to learn complex temporal patterns without excessively increasing the computational burden. This configuration harnessed the neural network's potential for capturing long-term dependencies of the time lag between surface and embedded layer temperature detection. To avoid overfitting in the model, an early stopping function with a patience value of 20 was adopted. The finalized hyperparameters include the implementation of an Adam optimizer, a learning rate of 0.0001, and a batch size of 12. The study by Nieduzak et al. provides further details regarding the ML architecture [31].

continued on page 29...

ACCE Award Winning Paper continued...

The ML temperature inference model proved effective in predicting surface temperatures based off embedded sensor readings in real time, producing an MAE and MAPE around 0.2°C and 0.5% respectively when tested on the four reserved realistic thermal runaway profiles. The results are shown in Figure 16, the left side presenting the real and predicted temperature curves, while the right section displays the error difference distribution histograms for each test case. The error difference distribution is narrowly concentrated with a mean close to zero, indicating strong predictive accuracy. This capability is crucial for the early detection of thermal runaway, particularly in applications where direct surface measurements are not feasible due to space constraints and sensor vulnerability.

Sensor Integrated Battery Enclosure Platform

The multifunctional battery enclosure reviewed in this study introduces a lightweight, self-sensing structure capable of providing decentralized monitoring of both structural and thermal states in EVs. Constructed from hybrid carbon and glass FRP composites, the enclosure achieves over 30% weight reduction compared to conventional aluminum housings. This reduction in mass directly contributes to improved vehicle efficiency and extended range which are key performance metrics for electrified transportation platforms.

Importantly, the sensing architecture is designed for real-world manufacturability and system integration. The carbon fiber sensor tows and embedded micro-temperature sensors are incorporated during standard composite preform and molding operations without the need for secondary bonding or surface mounting. Electrical connectivity is achieved through production-ready SOC terminals, which simplify the wiring layout and reduce points of mechanical failure. These design choices ensure compatibility with high-throughput automotive manufacturing environments.

All sensing outputs are processed in real time by a compact microcontroller system, leveraging inexpensive platforms such as the Arduino MKR series. This embedded system enables onboard signal acquisition, resistance tracking, temperature measurement, and ML inference without dependence on external processing infrastructure. As such, the enclosure serves as a standalone diagnostic system capable of integration with vehicle control systems or wireless telemetry networks. Crucially, the enclosure's embedded sensing suite operates independently from the main battery management system (BMS). This parallel functionality provides an added layer of safety redundancy, offering a self-contained means of early damage or thermal runaway detection. Even if the primary BMS becomes compromised or disabled during an adverse event, the enclosure's independent monitoring system remains functional, thereby avoiding a single point of failure. This decentralization enhances overall system robustness and enables more rapid responses to emergent thermal threats.

The enclosure is not only lighter and smarter but also modularly scalable, with the sensing architecture readily adaptable to different vehicle platforms. The demonstrated technologies are readily transferrable to various enclosure geometries,

continued on page 30...

This Issue:

ACCE Award Winning Paper continued...

including multi-module pack architectures. Additionally, the sensing algorithms are robust to noise and component variance, making them suitable for high-volume automotive manufacturing. This integration of materials, sensing, and intelligent data analytics within the enclosure structure itself represents a transformative step forward in EV battery system design, moving from passive protection to active condition awareness.

Conclusions

This paper presents a review of the design, fabrication, and validation of a multifunctional, self-monitoring FRP battery enclosure for electric vehicles, capable of delivering real-time structural and thermal diagnostics. The research unifies advanced composite materials, embedded sensing, finite element modeling, and ML to create a fully integrated, intelligent enclosure platform.

With respect to structural health, the FRP composite enclosure uses embedded carbon fiber tows to function as distributed piezoresistive sensors. Tensile, impact, and fatigue testing confirmed that these sensor tows provide accurate strain tracking, damage detection, and localization of impact events across large structural areas. A parallel-branch sensor network enabled low-cost damage localization using only a single terminal pair per sensing zone, with impact testing demonstrating localization errors under 3% across multiple scenarios. In addition to detecting new damage, the piezoresistive sensors exhibited progressive resistance increases that persist after loading, functioning as a reliable memory of accumulated damage over the composite's lifetime. This irreversible resistance shift correlates with fiber breakage and serves as a non-volatile record of the structure's mechanical history, enabling targeted inspection and repair. For fatigue monitoring, cyclic testing across multiple stress levels showed consistent resistance growth in the final 2–10% of life, offering a clear precursor to failure. An LSTM neural network was trained to interpret these resistance signals and predict RUL, successfully generalizing across test conditions without requiring stress or strain inputs. The model achieved robust predictive accuracy, demonstrating the feasibility of deploying resistance-only monitoring for long-term prognostics in EV battery enclosures.

Addressing thermal health, micro-temperature sensors were embedded within the composite structure during molding to monitor heat propagation under LIB thermal runaway conditions. Embedment of the temperature sensors minimizes cost, improves high-volume manufacturability, makes surface mounting steps unnecessary, accounts for space limitations, and provides sensor protection, but also introduces a time lag with respect to internal surface temperature measurement. To characterize this time lag, transient thermal experiments replicated both rapid (shock) and gradual (ramp-up) heating scenarios, while validated finite element simulations confirmed the anisotropic thermal response of the hybrid carbon-glass laminate. The measured and simulated composite responses showed excellent agreement, with a MAPE below 0.065% across all test cases. To compensate for the inherent time lag inherent to sub-surface temperature sensor readings, a machine learning temperature inference model was trained on

continued on page 31...

This Issue:

ACCE Award Winning Paper continued...

paired experimental and simulation data. This LSTM-based model predicted internal surface temperatures with a MAE of approximately 0.2°C and a MAPE of 0.5% when tested on realistic thermal runaway profiles derived from literature. These results demonstrate the system's ability to deliver accurate early-stage thermal diagnostics, even in the absence of direct surface temperature readings, enabling faster and more reliable thermal event detection within the battery enclosure.

Together, these sensing elements form a cohesive monitoring framework, interpreted by onboard microcontrollers in real time. The system requires no external instrumentation or surface-bonded sensors, enabling robust and scalable deployment across vehicle platforms. Moreover, the enclosure provides a level of autonomy in monitoring, functioning independently of the vehicle's primary BMS and offering early thermal runaway detection in critical failure scenarios.

In total, this work establishes a high-performance, lightweight, and production-compatible battery enclosure capable of both structural health monitoring and thermal anomaly detection. The enclosure advances EV safety standards by efficiently enabling predictive diagnostics and facilitating proactive maintenance. As EV adoption accelerates, such intelligent composite enclosures will be instrumental in achieving safe, reliable, and energy-efficient battery systems. Fully integrated production scale prototypes are currently being built for further testing. Future work may explore the integration of wireless communication modules, the implementation of more sensor types to detect other thermal runaway symptoms, and the adaptation to broader composite applications within the vehicle chassis. The modular nature of the sensing systems and embedded design establishes this platform as a versatile and scalable foundation for the next generation of smart, safety-oriented vehicle structures.

Acknowledgements

This research work is supported in part by the U.S Department of Energy (DOE) for a GM-led project under the contract DE-EE0009204.

Disclaimer: The information, data, or work presented herein was funded in part by an agency of the United States Government. Neither the United States Government nor any agency thereof, nor any of their employees, makes any warranty, express or implied, or assumes any legal liability or responsibility for the accuracy, completeness, or usefulness of any information, apparatus, product, or process disclosed, or represents that its use would not infringe privately owned rights. Reference herein to any specific commercial product, process, or service by trade name, trademark, manufacturer, or otherwise does not necessarily constitute or imply its endorsement, recommendation, or favoring by the United States Government or any agency thereof. The views and opinions of authors expressed herein do not necessarily state or reflect those of the United States Government or any agency thereof.

continued on page 32...

This Issue:

ACCE Award Winning Paper continued...

Bibliography

1. Diouf, B. and R. Pode, Potential of lithium-ion batteries in renewable energy. Renewable Energy, 2015. 76: p. 375-380.
2. Deng, D., Li-ion batteries: basics, progress, and challenges. Energy Science & Engineering, 2015. 3(5): p. 385-418.
3. Abaza, A., et al., Experimental study of internal and external short circuits of commercial automotive pouch lithium-ion cells. Journal of Energy Storage, 2018. 16: p. 211-217.
4. Dubaniewicz Jr, T.H. and J.P. DuCarme, Further study of the intrinsic safety of internally shorted lithium and lithium-ion cells within methane-air. Journal of loss prevention in the process industries, 2014. 32: p. 165-173.
5. Feng, X., et al., Characterization of penetration induced thermal runaway propagation process within a large format lithium ion battery module. Journal of Power Sources, 2015. 275: p. 261-273.
6. Xu, Y., et al., Mechanical properties and thermal runaway study of automotive lithium-ion power batteries. Ionics, 2022: p. 1-10.
7. Guo, R., et al., Mechanism of the entire overdischarge process and overdischarge-induced internal short circuit in lithium-ion batteries. Scientific reports, 2016. 6(1): p. 30248.
8. Lai, X., et al., Electrical behavior of over-discharge-induced internal short circuit in lithium-ion cells. Electrochimica Acta, 2018. 278: p. 245-254.
9. Ouyang, D., et al., Investigation of a commercial lithium-ion battery under overcharge/over-discharge failure conditions. RSC advances, 2018. 8(58): p. 33414-33424.
10. Lammer, M., A. Königseder, and V. Hacker, Holistic methodology for characterisation of the thermally induced failure of commercially available 18650 lithium ion cells. RSC advances, 2017. 7(39): p. 24425-24429.
11. Ma, W., et al., A mechanism-data driven resistance transfer algorithm for lithium-ion batteries and its application to thermal modeling. Journal of Energy Storage, 2024. 102: p. 114066.
12. Koch, S., K.P. Birke, and R. Kuhn, Fast thermal runaway detection for lithium-ion cells in large scale traction batteries. Batteries, 2018. 4(2): p. 16.
13. Dong, P., et al., Reliable and early warning of lithium-ion battery thermal runaway based on electrochemical impedance spectrum. Journal of the Electrochemical Society, 2021. 168(9): p. 090529.
14. Cai, T., et al., Detection of Li-ion battery failure and venting with Carbon Dioxide sensors. ETransportation, 2021. 7: p. 100100.
15. Koch, S., A. Fill, and K.P. Birke, Comprehensive gas analysis on large scale automotive lithium-ion cells in thermal runaway. Journal of Power Sources, 2018. 398: p. 106-112.
16. Brooke, L., Battle for the box, in Automotive Engineering. 2023, SAE International.
17. Lee, J., et al., Study of the effect of the aspect ratio of a cylindrical lithium-ion battery enclosure in an air-cooled thermal management system. Journal of Energy Storage, 2022. 45: p. 103684.
18. Demo, L.B., Damage Detection, Damage Localization, and Fatigue Life Prediction for Large-Area FRP Composites. 2024: Columbia University.
19. Demo, L.B., E.M. Tronci, and M.Q. Feng, Multifunctional fiber-reinforced polymer composites for damage detection and memory. Journal of Composites Science, 2023. 7(9): p. 383.
20. ASTM, A., D3039/D3039M-08 Standard Test Method for Tensile Properties of Polymer Matrix Composite Materials. ASTM International, 2014.

continued on page 33...

This Issue:

Sponsor the Newsletter

The Best Advertising Value in the Composites Industry

Contact: Teri Chouinard CBC, APR
Teri@IntuitGroup.com
See page 19 for more details

21. Demo, L.B., et al., Low-cost sensor-based damage localization for large-area monitoring of FRP composites. Smart Materials and Structures, 2024. 33(6): p. 065042.
22. Li, H., W. Zhou, and J. Ou, Study on electromechanical behavior of unidirectional carbon fibre sheet without epoxy resin matrix. Advances in Structural Engineering, 2004. 7(5): p. 437-445.
23. Kalashnyk, N., et al., Monitoring self-sensing damage of multiple carbon fiber composites using piezoresistivity. Synthetic Metals, 2017. 224: p. 56-62.
24. Demo, L.B., et al., Fatigue life prediction of self-sensing hybrid FRP composites via electrical resistance monitoring and LSTM neural network. Composite Structures, 2025: p. 119238.
25. Sensirion, STS4x Datasheet. 2022.
26. Zhang, H., et al., Experimental study of the anisotropic thermal conductivity of 2D carbon-fiber/epoxy woven composites. Composite Structures, 2021. 267: p. 113870.
27. Aitharaju, V., Material Properties of Acquired Composite Components. 2023.
28. Nieduzak, T.B., et al., Heat Transfer Model for Temperature-Sensing Polymer Composite EV Battery Enclosure. Composites Part B: Engineering, 2025: p. 112258.
29. Xie, H., et al. Lithium-Ion Battery Thermal Runaway Electro-Thermal Triggering Method and Toxicity Analysis. in IOP Conference Series: Earth and Environmental Science. 2021. IOP Publishing.
30. Noh, S.-H., Analysis of gradient vanishing of RNNs and performance comparison. Information, 2021. 12(11): p. 442.
31. Nieduzak, T.B., et al. Machine Learning Predictive Algorithm for Self-Sensing Electric Vehicle Battery Enclosure. in Smart Materials, Adaptive Structures and Intelligent Systems. 2024. American Society of Mechanical Engineers.

SPE COMPOSITES

This Issue:

THERMOSET TOPCON

WORLD'S LEADING THERMOSET TECHNOLOGY CONFERENCE & EXPO

Presented by SPE Thermoset Division

May 12 – 13, 2026 at the Monona Terrace in Madison, Wisconsin

SPONSOR AND/OR EXHIBIT & PRESENT AT – THE FUTURE OF THERMOSETS: AI AND EMERGING INDUSTRY INNOVATIONS

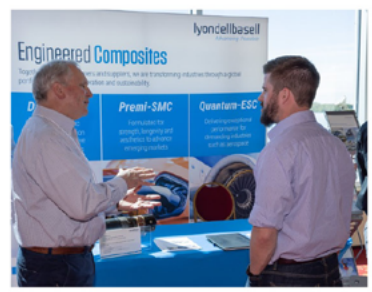

Advancements in AI are speeding developments in all industries and this year's event will feature keynotes and presentations on how the thermoset industry can benefit from this growing technology. Innovations in Materials, Additives, Molding, Testing, Applications, Business, Sustainability and More will also be featured. Abstracts due by February 28, 2026. Final Presentations due April 17, 2026. Please reach out ASAP as Limited Presentation and Exhibit spaces are available. Send Abstracts and Sponsorship and Exhibit inquiries to Teri Chouinard at Intuitgroup@gmail.com or call 248.701.8003, and Sean.Campbell@LYB.com or call 615.561.4234 and go to https://spethermosets.org/topcon/.

2025 SPONSORS

RECEPTION SPONSOR: plenco – PLASTICS ENGINEERING COMPANY

LUNCH SPONSOR: MBI MAR-BAL INCORPORATED

LUNCH SPONSOR: OMYA

BREAKFAST SPONSOR: IDI Composites International – idicomposites.com

BREAKFAST SPONSOR: LYB LyondellBasell

ALTA Performance Materials, AMERICAN COLORS INC., CENTURY, CORE, CIMBAR Performance Minerals, COMPOSITES ONE, fmtec solution, HUBER ENGINEERED MATERIALS, ICT MOLDING SOLUTIONS, Johns Manville, Lambient Technologies, McCLARIN, MP Molding Products, sensXPERT Technology by NETZSCH, OWENS CORNING, neptune NANO TECHNOLOGIES, PENN Compression Molding, Inc., TECHNICK PRODUCTS, PREMIX, HADLOCK, ZEHRCO-GIANCOLA COMPOSITES, INC., CompositesWorld, Plastics Technology, Plastics News, Urethanes Technology

Board of Directors

Dale Brosius
SPE Composites Director, Chair, and Chief Commercialization Officer, IACMI
Knoxville, TN
dbrosius@iacmi.org

Oleksandr G. Kravchenko, Ph.D.
SPE Composites Director, Past Chair, & Associate Professor, Dept. of Mechanical and Aerospace Engineering
Old Dominion University
Norfolk, VA
okravche@odu.edu

Mingfu Zhang, Ph.D.
SPE Composites Director, and Treasurer
Johns Manville
Sr. Research Manager, Corporate R&D
Littleton, CO
mingfu.zhang@jm.com

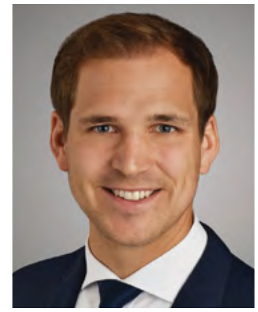

Christoph Kuhn, Ph.D.
SPE Composites Director, and Secretary
Volkswagen Group of America, Inc.
North American Engineering & Planning Center
Chattanooga, TN
christoph.kuhn@vw.com

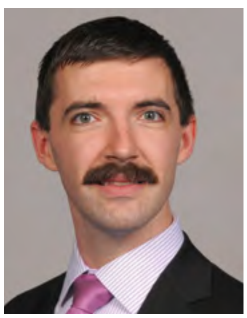

Ian Swentek, Ph.D.
SPE Composites Director, and Councilor, Applications Development Engineer Hexion
London, ON, Canada
Ian.Swentek@hexion.com

Creig Bowland
SPE Composites Director, President, Colorado Legacy Group,
Vandalia, MI
cbowland@coloradolegacy.com

John P. Busel, F. ACI
SPE Composites Director, & Intersociety Chair
V.P. Composites Growth Initiative
American Composites Manufacturers Association
Arlington, VA
jbusel@acmanet.org

Pritam Das
SPE Composites Director, Newsletter and Director of Technical Engineering,
Toray Composites Materials America (CMA)
Tacoma, WA
Pritam.das@toraycma.com

Frederick S. Deans
SPE Composites Director, Principal
Allied Composite Technologies, LLC
Rochester Hills, MI
fdeans@alliedcomptech.com

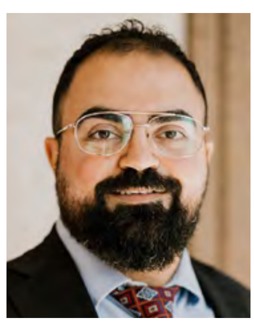

Hicham Ghossein, Ph.D.
SPE Composites Director, President & Founder of Endeavor Composites, Inc.
Knoxville, TN
hghossein@endeavorcomposites.com

Jack Gillespie, Ph.D.
SPE Composites Director, Phillips Emeritus Professor
Center for Composite Materials
University of Delaware
Newark, DE
gillespi@udel.edu

Vipin Kumar, Ph.D.
SPE Composites Director and Award Chair,
R&D Staff Member, Manufacturing Science Division,
Oak Ridge National Laboratory, Knoxville, TN
kumarvi@ornl.gov

SPONSOR LINKS

AOC Trusted Solutions
BASF We create chemistry
DSC Consumables incorporated Est. 2012 Austin, MN
Michelman
Mitsubishi Chemical Group
MP Molding Products
vartega

Board of Directors continued...

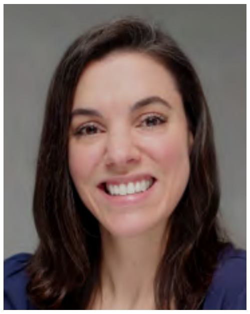

Amanda Nummy
SPE Composites Director, and Sr. Polymer Materials Engineer
HATCI, Superior Township, MI
anummy@hatci.com

Srikanth Pilla, Ph.D.
SPE Composites Director, and Professor & Director at Center for Composite Materials
University of Delaware
Newark, DE
spilla@udel.edu

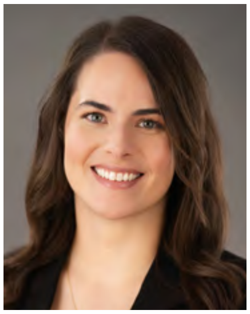

Dr. Sara Simon
SPE Composites Director, Sector Manager Polymers, NETZSCH, Selb, DE.
sara.simon@netzsch.com

Antoine Rios, Ph.D.
SPE Composites Director, Finance Chair,
The Madison Group
Madison, WI
Antoine@madisongroup.com

Uday Vaidya, Ph.D.
SPE Composites Director, and Education Chair
Professor in Mechanical, Aerospace & Biomedical Engineering
Chief Technology Officer (CTO), IACMI
University of Tennessee
Knoxville, TN
uvaidya@utk.edu

Pritesh Yeole, Ph.D.
SPE Composites Director, Research Associate in Advanced Composites Manufacturing
Fibers and Composites Manufacturing Facility
University of Tennessee
Knoxville, TN
pyeole@vols.utk.edu

This Issue:

Sponsor the Newsletter

The best advertising value in the Composites Industry

- **Support your SPE Composites Division**
- **Reach 1,000 Composites Professionals 3 Times a year via the E-Newsletter**
- **Maximize your exposure to the customers & the trade**

Contact Teri Chouinard CBC, APR for more info intuitgroup@gmail.com
See page 19 for more details